1-1-2014

Conductivity and oxygen reduction activity changes in lanthanum strontium manganite upon low-level chromium substitution

George Tsekouras
University of Wollongong, georget@uow.edu.au

Artur Braun
Swiss Federal Laboratories for Materials Science and Technology

Conductivity and oxygen reduction activity changes in lanthanum strontium manganite upon low-level chromium substitution

Abstract

On the timescale of solid oxide fuel cell (SOFC) system lifetime requirements, the thermodynamically predicted low-level substitution of chromium on the B-site of (La,Sr)MnO_3 could be a source of cathode degradation underlying more overt and well-known chromium poisoning mechanisms. To study this phenomenon in isolation, electronic conductivity (σ) and electrochemical oxygen reduction activity of the $(La_{0.8}Sr_{0.2})_{0.98}Cr_xMn_{1-x}O_3$ model series (x = 0, 0.02, 0.05 or 0.1) were measured in air between 850 and 650 °C. Depending on the extent of chromium substitution and the measurement temperature, electrochemical impedance spectroscopy (EIS) results could be deconvoluted into a maximum of three contributions reflecting possible limiting processes such as oxide ion transport and dissociative adsorption. Chromium substitution resulted in lowered σ (from 174 S cm^{-1} (x = 0) to 89 S cm^{-1} (x = 0.1) at 850 °C) and a steady rise in associated activation energy (E_a) (from 0.105 ± 0.001 eV (x = 0) to 0.139 ± 0.001 eV (x = 0.1)). From EIS analyses, ohmic and polarisation resistances increased, whilst Ea for the overall oxygen reduction reaction also increased from 1.39 ± 0.04 eV (x = 0) to 1.48-1.54 ± 0.04 eV upon chromium substitution.

Keywords

level, conductivity, oxygen, reduction, activity, changes, chromium, lanthanum, substitution, strontium, manganite, upon, low

Disciplines

Engineering | Physical Sciences and Mathematics

Publication Details

Tsekouras, G. & Braun, A. (2014). Conductivity and oxygen reduction activity changes in lanthanum strontium manganite upon low-level chromium substitution. Solid State Ionics, 266 19-24.

Conductivity and oxygen reduction activity changes in lanthanum strontium manganite upon low-level chromium substitution

George Tsekouras* and Artur Braun

Laboratory for High Performance Ceramics

Swiss Federal Laboratories for Materials Science and Technology

Überlandstrasse 129

Dübendorf 8600

Switzerland

*E: george.tsekouras@empa.ch

*T: +41 (0)58 765 4952

Keywords: solid oxide fuel cell; lanthanum strontium manganite; chromium poisoning; electronic conductivity; electrochemical impedance spectroscopy

Abstract

On the timescale of solid oxide fuel cell (SOFC) system lifetime requirements, the thermodynamically predicted low-level substitution of chromium on the B-site of $(La,Sr)MnO_3$ could be a source of cathode degradation underlying more overt and well-known chromium poisoning mechanisms. To study this phenomenon in isolation, electronic conductivity (σ) and electrochemical oxygen reduction activity of the $(La_{0.8}Sr_{0.2})_{0.98}Cr_xMn_{1-x}O_3$ model series (x = 0, 0.02, 0.05 or 0.1) were measured in air between 850 and 650 °C. Depending on the extent of chromium substitution and the measurement temperature, electrochemical impedance spectroscopy (EIS) results could be deconvoluted into a maximum of three contributions

reflecting possible limiting processes such as oxide ion transport and dissociative adsorption. Chromium substitution resulted in lowered σ (from 174 S cm^{-1} (x = 0) to 89 S cm^{-1} (x = 0.1) at 850 °C) and a steady rise in associated activation energy (E_a) (from 0.105 ± 0.001 eV (x = 0) to 0.139 ± 0.001 eV (x = 0.1)). From EIS analysis, ohmic and polarisation resistances increased, whilst E_a for the overall oxygen reduction reaction also increased from 1.39 ± 0.04 eV (x = 0) to 1.48–1.54 ± 0.04 eV upon chromium substitution.

1. Introduction

Solid oxide fuel cells (SOFCs) are promising for the distributable and efficient conversion of chemical energy (e.g. from natural gas, biogas, liquefied petroleum gas) to electrical energy, and could thus play an important role in lowering greenhouse gas emissions. However, SOFCs can suffer from a number of stability problems, including chromium poisoning of the widely employed cathode based on the perovskite oxide (La,Sr)MnO_3 by chromium-containing metallic alloy interconnects. Numerous studies (e.g. [1-20]) have considered the severity of chromium poisoning of (La,Sr)MnO_3-based cathodes depending on whether the SOFC is operated under load or is held at open-circuit, whether the air supplied to the cathode is dry or humidified, and depending on the interconnect metallic alloy used (Inconel 600, Cr5Fe1Y_2O_3, Crofer22APU, RA446, 17-4 stainless steel, AISI 441, SUS430, ITM or ZMG232).

Chromium poisoning of (La,Sr)MnO_3-based SOFC cathodes includes the initial formation of $Cr_2O_{3(s)}$ on the interconnect surface, volatilisation of $Cr_2O_{3(s)}$ to $CrO_{3(g)}$ and $CrO_2(OH)_{2(g)}$, reaction of chromium species with (La,Sr)MnO_3, and deposition of volatile chromium species as $Cr_2O_{3(s)}$ at triple-phase-boundary (TPB) active sites. Regarding the reaction of chromium species with (La,Sr)MnO_3, formation of the spinel $(Cr,Mn)_3O_4$ is generally observed in chromium poisoning experiments. By extension, the formation of $(Cr,Mn)_3O_4$ is accompanied by the formation of (La,Sr)$(Cr,Mn)O_3$ according to the equations below [2], which describe the reaction of (La,Sr)MnO_3 with solid (1) or gaseous (2) chromium species:

$$1.5\ Cr_2O_{3(s)} + 3\ (La,Sr)MnO_3 \rightarrow 3\ (La,Sr)(Cr_{1-y}Mn_y)O_3 + (Cr_yMn_{1-y})_3O_4 + 0.25\ O_2 \qquad (1)$$

$$3\ CrO_{3(g)} + 3\ (La,Sr)MnO_3 \rightarrow 3\ (La,Sr)(Cr_{1-y}Mn_y)O_3 + (Cr_yMn_{1-y})_3O_4 + 2.5\ O_2 \quad (2)$$

Another possible route to $(La,Sr)(Cr,Mn)O_3$ was raised in a study considering the thermodynamics of chromium poisoning in SOFC cathodes [21], where it was predicted that at typical SOFC operating temperatures chromium can be dissolved into $(La,Sr)MnO_3$ without forming other phases and with the corresponding advent of A-site deficiency according to:

$$(La_{0.8}Sr_{0.2})MnO_3 + 0.1\ CrO_{3(g)} \rightarrow 1.1\ (La_{0.8}Sr_{0.2})_{0.909}(Cr_{0.091}Mn_{0.909})O_3 \quad (3)$$

Although thermodynamically predicted, chromium substitution into the perovskite lattice of $(La,Sr)MnO_3$ has not been observed during the course of chromium poisoning experiments, suggesting slow kinetics [21]. Assuming slow kinetics, the non-observation of chromium-substituted $(La,Sr)MnO_3$ is not surprising considering that exposure times in all but one (Menzler *et al* [13], 8,000 h exposure time) of the above-cited chromium poisoning studies were ≤ 3,000 h and therefore short compared to SOFC system lifetime requirements, which exceed 40,000 h [20, 22]. Moreover, it would be nearly impossible to distinguish any chromium-substituted $(La,Sr)MnO_3$ formed from $(La,Sr)MnO_3$ using the common technique of X-ray diffractometry (XRD), since these materials are isostructural on account of the fact that the ionic radii [23] of VI-coordinate (high spin) Mn^{3+} (0.645 Å) and Cr^{3+} (0.615 Å) are similar. Considering that SOFC system lifetime requirements are quite long, the thermodynamically predicted and seemingly slow process of chromium-substituted $(La,Sr)MnO_3$ formation could be a source of performance degradation underlying more overt and well-known chromium poisoning mechanisms.

To study in isolation the possible degradation of SOFC cathode performance due to the reaction of chromium species with $(La,Sr)MnO_3$, the present study considers the electronic conductivity (σ) and electrochemical oxygen reduction activity of $(La,Sr)MnO_3$ into which chromium was systematically substituted at low levels (≤ 0.1) for manganese on the B-site. Regarding electronic properties, these materials differ

considerably compared to widely utilised LSCM SOFC electrode materials, such as the $La_{0.75}Sr_{0.25}Cr_{0.5}Mn_{0.5}O_3$ composition reported by Tao and Irvine [24], since the low-level concentrations of chromium on the B-site are well below the percolation threshold (0.33). Electronic conductivity was considered using the results of electrical conductivity measurements, since the ionic conductivity of $(La,Sr)MnO_3$ is known to be several orders of magnitude lower in comparison [25]. In order to achieve the aims of the present study the $(La_{0.8}Sr_{0.2})_{0.98}Cr_xMn_{1-x}O_3$ model series (x = 0, 0.02, 0.05 or 0.1) was investigated in air over the temperature range 850-650 °C. The somewhat modest maximum extent of chromium substitution (x = 0.1) was chosen since equation (3) [21] suggests that a substitution level approaching 10 % is thermodynamically possible.

2. Experimental

The $(La_{0.8}Sr_{0.2})_{0.98}Cr_xMn_{1-x}O_3$ model series was prepared *via* solid state synthesis using stoichiometric amounts of La_2O_3, $SrCO_3$, Cr_2O_3 and Mn_2O_3. Prior to accurate weighing of precursor powders, La_2O_3 was decarbonised at 900 °C, while $SrCO_3$, Cr_2O_3 and Mn_2O_3 were dried at 300 °C. Powders were mixed in a mortar and pestle with acetone and dried before calcination at 1000 °C for 12 h. Calcined powder mixtures were ground in a mortar and pestle followed by uniaxial pressing under 150 MPa load into pellets that were fired at 1300 °C for 12 h. Fired pellets were ground in a mortar and pestle and resultant powders planetary ball-milled in isopropanol using Ø 3 mm zirconia balls at 400 rpm for 1 h. Recovered powders were uniaxially pressed, fired and milled as above. An additional planetary ball-milling step in isopropanol was carried out using Ø 1 mm zirconia balls at 400 rpm for 0.5 h in order to lower particle size and therefore improve sinterability of final powders. Room temperature powder XRD was performed on a PANalytical X'Pert Pro diffractometer operated in reflection mode using Cu-Kα_1 radiation, 2θ range 20-80°, 0.017° step and 1 h scan duration.

Pellets for van der Pauw electrical conductivity measurements were prepared by mixing ~ 3.3 g $(La_{0.8}Sr_{0.2})_{0.98}Cr_xMn_{1-x}O_3$ powder, 3x drops of KD-6 liquid polymeric surfactant and acetone in a mortar and pestle. Dried mixtures were uniaxially pressed under 150 MPa load into pellets that were fired at 1300 °C for 12 h, yielding pellets with 78-84 % relative density. Measurements were performed under constant air flow

on cooling from 850 °C to 650 °C using Pt wire connections, a ProboStat^{TM} unit (NorECs AS) inserted into the hot zone of a vertical furnace, and a multimeter (Keithley 2750).

Symmetrical cells for electrochemical oxygen reduction activity measurements were prepared in triplicate and based on a dense 8 mol.% yttria-stabilsed zirconia (YSZ) electrolyte with electrodes on either side composed of active composite (La,Sr)(Cr,Mn)O_3/YSZ and current-collecting pure (La,Sr)(Cr,Mn)O_3 layers. Composite (La,Sr)(Cr,Mn)O_3/YSZ active layers were used to make the experiments technologically relevant and to minimise possible microstructural variation brought about by any changes in the sinterability of (La,Sr)MnO_3 upon chromium substitution. The architecture of symmetrical cells was (La,Sr)(Cr,Mn)O_3/((La,Sr)(Cr,Mn)O_3/YSZ)//YSZ//((La,Sr)(Cr,Mn)O_3/YSZ)/(La,Sr)(Cr,Mn)O_3. The extent of chromium substitution in the active and current collecting layers was matched for each value of *x* in the $(La_{0.8}Sr_{0.2})_{0.98}Cr_xMn_{1-x}O_3$ model series. Dense YSZ pellets with Ø 20 mm and 2 mm thickness were prepared by uniaxially pressing 3.6 g commercial YSZ powder under 35 MPa load followed by firing at 1450 °C for 12 h. For each composite (La,Sr)(Cr,Mn)O_3/YSZ (50:50 by weight) and pure (La,Sr)(Cr,Mn)O_3 screen-printing ink 1.0 g ceramic was dispersed in acetone with 2 wt.% KD-1 dispersant using an ultrasonic probe for 10 min. To this dispersion was added 0.43 g vehicle consisting of 5 wt.% poly(vinyl butyrate) in terpineol, giving a ceramic:vehicle weight ratio of 70:30. The mixture was magnetically stirred at room temperature overnight to evaporate the acetone and yield the final ink. Composite (La,Sr)(Cr,Mn)O_3/YSZ and pure (La,Sr)(Cr,Mn)O_3 inks were each screen-printed through a 325 mesh to 2x layers thickness in Ø 12 mm disc shape on either side of dense YSZ pellets with drying between the application of layers. Symmetrical cells were fired at 1000 °C for 2 h. Cross-sectional scanning electron microscopy (SEM) of symmetrical cells indicated active and current-collecting layer thicknesses ranging between 20-24 μm and 9-12 μm, respectively. To assist current collection, gold paste was applied to symmetrical cells in a radial pattern and fired at 900 °C for 0.5 h. A control Au/YSZ/Au symmetrical cell was also prepared to allow the contribution of the YSZ electrolyte, wires and contacts to ohmic resistance (R_s) to be subtracted from the results obtained for (La,Sr)(Cr,Mn)O_3-based symmetrical cells.

Electrochemical oxygen reduction activity measurements on triplicate symmetrical cells were performed under constant air flow on cooling from 850 °C to 650 °C using Pt wire connections, a ProboStat^{TM} unit (NorECs AS) inserted into the hot zone of a vertical furnace, a frequency response analyser (Solartron SI 1260), an electrochemical interface (Solartron 1296) and SMaRT v3.0.1 software (Solartron). Electrochemical impedance spectroscopy (EIS) was carried out using 100 mV AC perturbation, 1 MHz – 0.2 Hz frequency range, and 3 cycles integration. The results of EIS measurements were analysed using ZView v2.80 software (Scribner Associates).

3. Results and Discussion

3.1. X-ray diffractometry

The XRD patterns of $(La_{0.8}Sr_{0.2})_{0.98}Cr_xMn_{1-x}O_3$ powders prepared in air *via* solid state synthesis are presented in Fig. 1. Compositions were isostructural single phase perovskites with respect to XRD analysis, while the observed peak splitting was consistent with rhombohedral crystal symmetry.

3.2. Electronic conductivity

The substitution of Sr^{2+} for La^{3+} on the A-site of $LaMnO_3$ is described by equation (4). In air, the lower oxidation state of Sr^{2+} compared to La^{3+} is electrically compensated *via* oxidation of the manganese B-site cation from 3+ to 4+. The $Mn_{Mn}^{\bullet}$ charge carrier makes (La,Sr)MnO_3 an electronic conductor.

$$2\,SrO + 2\,Mn_{Mn}^{x} + 1/2\,O_2 \rightarrow 2\,Sr'_{La} + 2\,Mn_{Mn}^{\bullet} + 3\,O_O^{x} \quad (4)$$

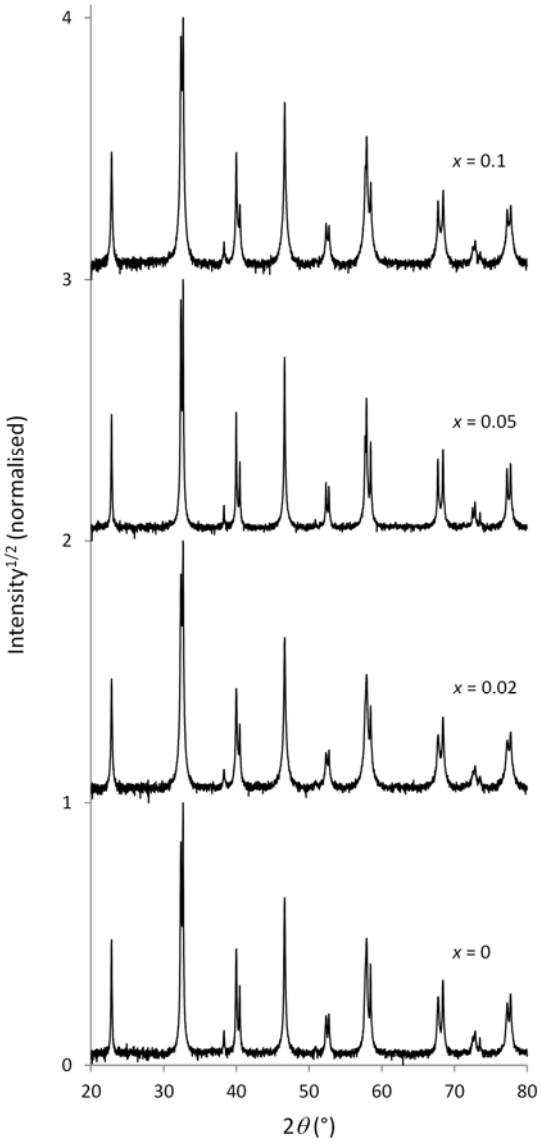

Fig. 1. X-ray diffraction patterns of $(La_{0.8}Sr_{0.2})_{0.98}Cr_xMn_{1-x}O_3$ powders prepared in air *via* solid state synthesis, with extent of chromium substitution (x) as indicated.

The electronic conductivity (σ) of $(La_{0.8}Sr_{0.2})_{0.98}Cr_xMn_{1-x}O_3$ pellets measured in air between 850-650 °C using the van der Pauw method is shown in Fig. 2. Electronic conductivity followed a small polaron hopping mechanism [25], while the data presented in Fig. 2 was fitted using equation (5), where T = temperature, E_a = activation energy and R = gas constant.

$$\sigma T = \sigma_0 \exp(-E_a/RT) \quad (5)$$

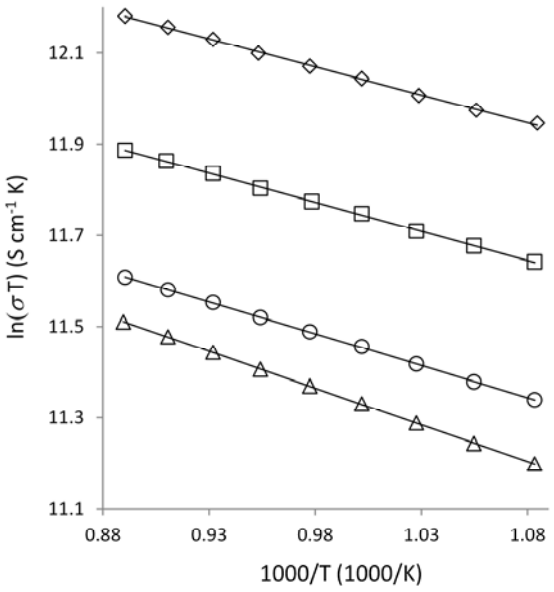

Fig. 2. Electronic conductivity (σ) of $(La_{0.8}Sr_{0.2})_{0.98}Cr_xMn_{1-x}O_3$ pellets measured in air between 850-650 °C using the van der Pauw method. (◊) x = 0, (□) x = 0.02, (○) x = 0.05, (Δ) x = 0.1.

Low-level chromium substitution for manganese on the B-site of $(La_{0.8}Sr_{0.2})_{0.98}MnO_3$ resulted in a steady lowering of electronic conductivity, similar to that reported previously for low-level chromium-substituted $La_{0.92}Sr_{0.08}MnO_3$ [26]. For example, σ values at 850 °C of 174, 129, 98 and 89 S cm^{-1} were measured for x values of 0, 0.02, 0.05 and 0.1, respectively. In a real SOFC cathode such a lowering of electronic conductivity would result in raised ohmic losses and interfere with the supply of electrons to active sites for the oxygen reduction reaction (ORR), which would in turn both result in degradation of SOFC performance. However, it is reasonable to assume that the formation of more resistive $(La,Sr)(Cr,Mn)O_3$ in a real SOFC cathode would be largely limited to grain surfaces, and that the transport of electrons would therefore occur predominantly through more conductive $(La,Sr)MnO_3$ grain cores. In turn, this suggests that the degradation of a real $(La,Sr)MnO_3$ SOFC cathode upon reaction with chromium species due to lowered electronic conductivity would not be as extensive as inferred by the results presented in Fig. 2.

Electronic conductivity is proportional to the product of the concentration and mobility of charge carriers ($[Mn_{Mn}^{\bullet}]$ and μ, respectively). Charge carrier concentration is one of the constants that constitute the pre-exponential term σ_0 in equation (5) [25]. Therefore, to gauge variation in $[Mn_{Mn}^{\bullet}]$ with the extent of chromium substitution in the $(La_{0.8}Sr_{0.2})_{0.98}Cr_xMn_{1-x}O_3$ model series, ln σ_0 values from Fig. 2 were plotted against x (Fig. 3). Only a slight decrease in ln σ_0 values with x was observed, suggesting that $[Mn_{Mn}^{\bullet}]$ was largely unchanged with extent of chromium substitution. Furthermore, $[Mn_{Mn}^{\bullet}]$ in $(La,Sr)MnO_3$ is not expected to change with chromium substitution since manganese B-sites have a lower small polaron site energy compared to chromium B-sites [27], suggesting that charge compensation for the replacement of La^{3+} by Sr^{2+} on the A-site would occur exclusively through the formation of $Mn_{Mn}^{\bullet}$. This has been confirmed by X-ray absorption near edge structure spectroscopy of $La_{1-x}Sr_xCr_{0.5}Mn_{0.5}O_3$ compositions [27], where the Cr K edge did not deviate with extent of strontium substitution and was consistent with Cr^{3+}, while the Mn K edge shifted upon strontium substitution indicating compensation at the manganese B-site. Based on experimental results obtained here and with reference to the literature, the observed steady lowering of electronic conductivity with x for the $(La_{0.8}Sr_{0.2})_{0.98}Cr_xMn_{1-x}O_3$ model series may therefore be attributed to lowered μ, which in turn may be attributed to a reduction in the number of available small polaron hopping manganese B-sites.

E_a for electronic conductivity calculated from the slopes of the $\ln(\sigma T)$ *vs.* 1000/T plots in Fig. 2 increased with extent of chromium substitution in the $(La_{0.8}Sr_{0.2})_{0.98}Cr_xMn_{1-x}O_3$ model series, with values of 0.105, 0.110, 0.121 and 0.139 eV (± 0.001 eV) calculated for x = 0, 0.02, 0.05 and 0.1, respectively. The plot of these values in Fig. 3 shows a significant and steady rise in E_a with increasing x, indicative of a raised barrier to thermally activated hopping of charge carriers. This may be attributed, as above, to a lowering of the number of available manganese B-sites for small polaron hopping.

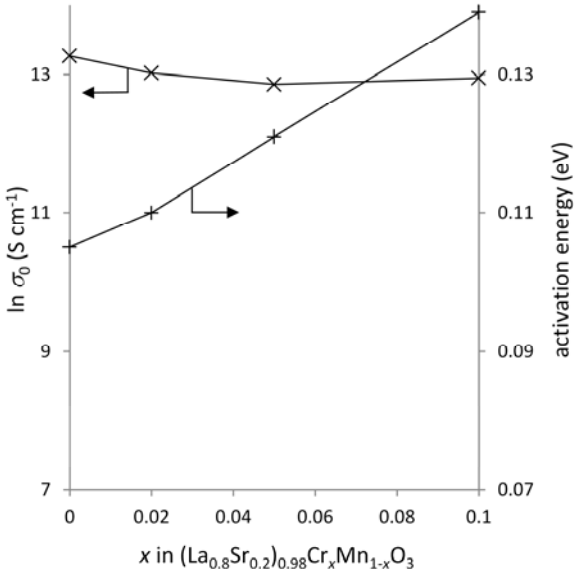

Fig. 3. ln σ_0 (×) and activation energy (+) from Fig. 2 ln(σT) *vs.* 1000/T plots for the $(La_{0.8}Sr_{0.2})_{0.98}Cr_xMn_{1-x}O_3$ model series plotted against extent of chromium substitution (*x*). Error bars (not shown) smaller than symbols.

3.3. Electrochemical oxygen reduction activity

For each value of *x* in the $(La_{0.8}Sr_{0.2})_{0.98}Cr_xMn_{1-x}O_3$ model series, at least two of the triplicate symmetrical cells exhibited near overlapping impedance spectra at all measurement temperatures. From these, one was randomly selected for presentation and detailed fitting as described below.

EIS analyses gauging the activity of the $(La_{0.8}Sr_{0.2})_{0.98}Cr_xMn_{1-x}O_3$ model series towards electrochemical oxygen reduction were interpreted in accordance with the classification put forward by Jørgensen and Mogensen in 2001 [28] regarding processes on composite (La,Sr)MnO_3/YSZ electrodes. Based upon a thorough review of literature regarding the EIS analysis of (La,Sr)MnO_3/YSZ electrodes, as well as new experimental data, Jørgensen and Mogensen identified processes "A,B", "C", "D" and "E". Characteristic relaxation frequency (ν^*) values observed in this study were consistent with processes A,B and C, which relate to transport of oxide ions and/or oxygen intermediates across (La,Sr)MnO_3/YSZ interfaces and through the YSZ phase of the

composite, and to dissociative adsorption, transfer of species at TPBs, and surface diffusion, respectively. Process D, related to gas diffusion impedance, was also observed in this study, however was not taken into account since the magnitude of this process was observed to be invariant with respect to *x* and temperature. Process E, related to low frequency induction, was not observed in this study.

In addition to the deconvolution of process A,B from process C, it was found that process C could be further separated into two processes denoted here as C_1 and C_2. EIS spectra were therefore fitted using the equivalent circuit depicted in Fig. 4, where: L = inductance; R_s = ohmic resistance; $R_{A,B}$, R_{C_1} and R_{C_2} = polarisation resistances corresponding to processes A,B, C_1 and C_2, respectively; and $CPE_{A,B}$, CPE_{C_1} and CPE_{C_2} = constant phase elements corresponding to processes A,B, C_1 and C_2, respectively. L and R_s elements and the R_{C_2}//CPE_{C_2} unit were used in every fit, while the number of R//CPE units invoked was kept to a minimum. The R_{C_1}//CPE_{C_1} unit was used for all values of *x* and for all temperatures except for *x* = 0 and T = 850, 825 °C. The $R_{A,B}$//$CPE_{A,B}$ unit was used for all values of *x* and T = 750-650 °C. Where possible, the ability to deconvolute processes A,B, C_1 and C_2 was based on a minimum order-of-magnitude separation of associated relaxation frequencies. This is demonstrated in Table 1, which shows ν^* values observed at 750 °C for processes A,B, C_1 and C_2 depending on *x*. Fig. 5 shows an example deconvolution and overall fitting of EIS data measured in air at 650 °C for a symmetrical cell based on $(La_{0.8}Sr_{0.2})_{0.98}Cr_{0.1}Mn_{0.9}O_3$, using the full equivalent circuit depicted in Fig. 4.

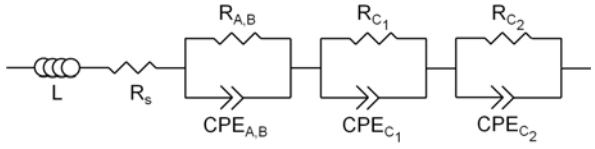

Fig. 4. Equivalent circuit used to fit electrochemical impedance spectroscopy data obtained for symmetrical cells based on the $(La_{0.8}Sr_{0.2})_{0.98}Cr_xMn_{1-x}O_3$ model series.

Table 1. Relaxation frequencies (measured at 750 °C) and activation energies corresponding to oxygen reduction reaction processes A,B, C_1 and C_2 for symmetrical cells based on the $(La_{0.8}Sr_{0.2})_{0.98}Cr_xMn_{1-x}O_3$ model series.

process	relaxation frequency (Hz)				activation energy (eV)			
	x = 0	x = 0.02	x = 0.05	x = 0.1	x = 0	x = 0.02	x = 0.05	x = 0.1
A,B	1.5×10^4	1.6×10^4	2.4×10^4	2.3×10^4	1.74 ± 0.04	1.70 ± 0.08	1.50 ± 0.02	2.00 ± 0.05
C_1	6.8×10^2	2.7×10^2	3.5×10^2	4.3×10^2	1.62 ± 0.05	1.50 ± 0.04	1.61 ± 0.06	1.72 ± 0.06
C_2	3.5×10^1	2.5×10^1	3.1×10^1	2.0×10^1	0.94 ± 0.03	1.29 ± 0.04	1.26 ± 0.02	1.23 ± 0.03

Fig. 6 compares EIS analyses of symmetrical cells based on all $(La_{0.8}Sr_{0.2})_{0.98}Cr_xMn_{1-x}O_3$ model series compositions measured in air at 850 °C. Cross-sectional SEM (not shown) of symmetrical cells indicated qualitatively similar microstructures independent of *x*, such that EIS analyses could be interpreted in terms of changes in chemistry. The main distinction observed in Fig. 6 was the lower R_s and polarisation resistance (R_p) of unsubstituted (La,Sr)MnO_3 (x = 0) compared to the results observed for chromium-substituted compositions (x = 0.02, 0.05 or 0.1). The higher R_s of chromium-substituted compositions was broadly consistent with the steady decrease in electronic conductivity associated with substitution (Fig. 2), in conjunction with the fact that the radial pattern of gold paste employed only assisted current collection in symmetrical cells, meaning that lateral resistance of pure (La,Sr)(Cr,Mn)O_3 current collecting layers was a factor in determining R_s. The higher R_p of chromium-substituted compositions was likely the result of interfered supply of electrons to TPBs and retardation of ORR processes following the substitution of catalytically active Mn B-site cations with less catalytically active Cr cations. Translated to a real cathode, the increases in R_s and R_p observed here due to chromium substitution for manganese in (La,Sr)MnO_3 would result in SOFC performance degradation.

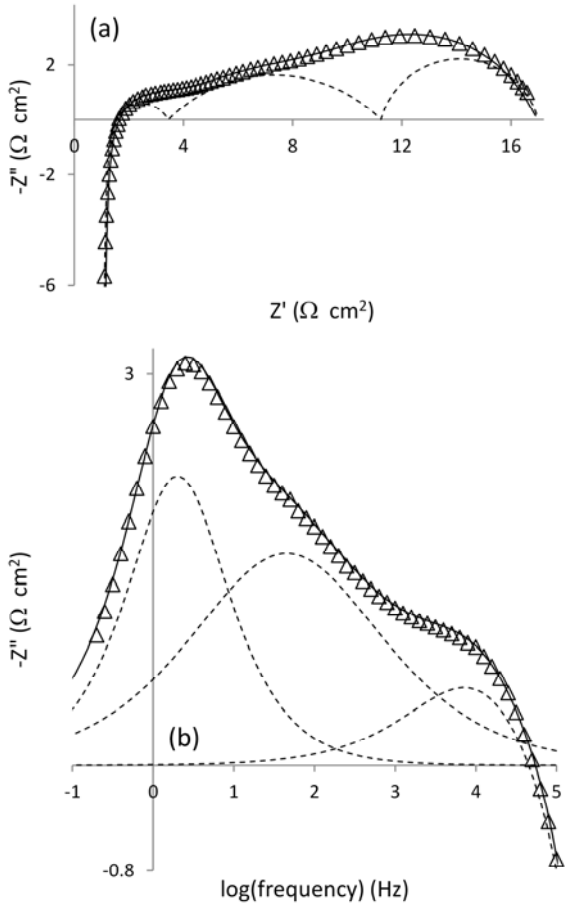

Fig. 5. Example deconvolution and overall fitting of (a) Nyquist and (b) Bode plots measured in air at 650 °C for a symmetrical cell based on $(La_{0.8}Sr_{0.2})_{0.98}Cr_{0.1}Mn_{0.9}O_3$. (Δ) experimental data, (---) individual components of fit, (—) overall fit. Contribution of YSZ electrolyte, wires and contacts to ohmic resistance subtracted from data in (a).

A full comparison of the electrochemical oxygen reduction activity of all $(La_{0.8}Sr_{0.2})_{0.98}Cr_xMn_{1-x}O_3$ model series compositions in air over the temperature range 850-650 °C is presented in Fig. 7, which shows separately the temperature dependencies of processes A,B, C_1 and C_2, and of the overall ORR.

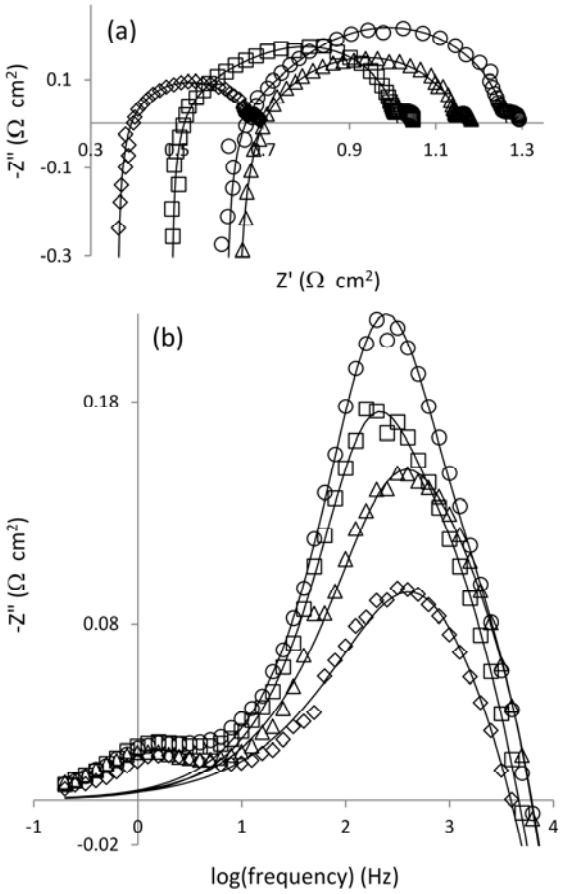

Fig. 6. Electrochemical impedance spectroscopy analysis in air at 850 °C of symmetrical cells based on $(La_{0.8}Sr_{0.2})_{0.98}Cr_xMn_{1-x}O_3$ model series. (a) Nyquist plot. (b) Bode plot. (◊) x = 0, (□) x = 0.02, (○) x = 0.05, (Δ) x = 0.1. Overall fits indicated by solid lines. Contribution of YSZ electrolyte, wires and contacts to ohmic resistance subtracted from data in (a).

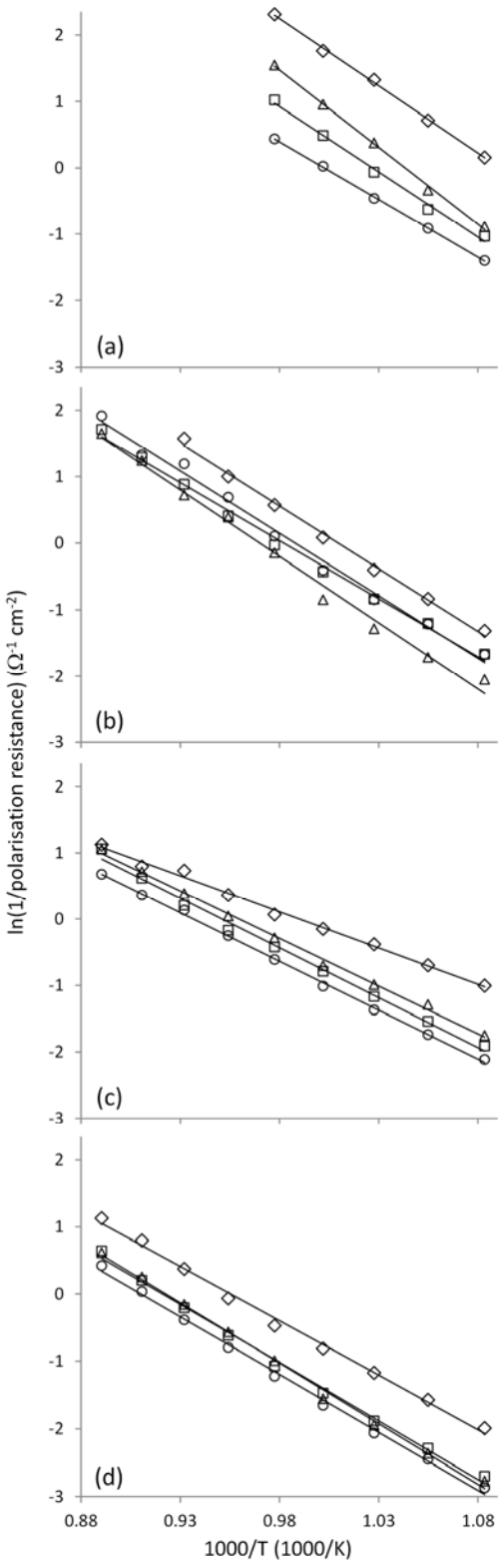

Fig. 7. Electrochemical oxygen reduction activity of $(La_{0.8}Sr_{0.2})_{0.98}Cr_xMn_{1-x}O_3$ model series in air over the temperature range 850-650 °C. (a) process A,B, (b) process C_1, (c) process C_2, (d) overall oxygen reduction reaction. (◊) x = 0, (□) x = 0.02, (○) x = 0.05, (Δ) x = 0.1.

$R_{A,B}$, in part associated with the transport of oxide ions and/or oxygen intermediates across (La,Sr)MnO_3/YSZ interfaces, made up the smallest contribution to total R_p for all compositions. Fig. 7(a) indicates that $R_{A,B}$ for unsubstituted (La,Sr)MnO_3 was considerably lower compared to chromium-substituted compositions, while no pattern in associated E_a values (Table 1) could be identified. R_{C_1}, which may be related to dissociative adsorption, transfer of species at TPBs, or surface diffusion, was lower for unsubstituted (La,Sr)MnO_3 compared to chromium-substituted compositions (Fig. 7(b)). E_a values associated with process C_1 (Table 1) for x = 0, 0.05 and 0.1 compositions were equal within experimental error, while that for the x = 0.02 composition was slightly lower in comparison. In the absence of chromium substitution, E_a for process C_2 was lower by between 0.29-0.35 eV (Table 1), which in part led to similar R_{C_2} values for all compositions at higher temperatures, while at lower temperatures R_{C_2} values for the x = 0 composition were substantially lower compared to x = 0.02, 0.05 and 0.1 compositions (Fig. 7(c)).

The temperature dependence of the overall ORR presented in Fig. 7(d) shows a clear distinction between the considerably lower total R_p of unsubstituted (La,Sr)MnO_3 compared to the rather similar results observed for chromium-substituted compositions. This was a manifestation of the consistently lower R_p values observed for unsubstituted (La,Sr)MnO_3 with regard to each of the individual processes A,B, C_1 and C_2, as described in Fig. 7(a-c). Thus chromium substitution on the B-site of (La,Sr)MnO_3 interfered with ORR processes including possibly transport of oxide ions and/or oxygen intermediates across (La,Sr)MnO_3/YSZ interfaces, dissociative adsorption, transfer of species at TPBs, and surface diffusion. Overall ORR E_a values for x = 0, 0.02, 0.05 and 0.1 compositions were 1.39 ± 0.04, 1.49 ± 0.04, 1.48 ± 0.03 and 1.54 ± 0.03 eV, respectively. That is, the overall ORR E_a value for unsubstituted (La,Sr)MnO_3 was between 0.09-0.15 eV lower compared to chromium substituted compositions, while E_a values for x = 0.02, 0.05 and 0.1 compositions were equal within experimental error. Overall ORR E_a values determined in this study were similar to those reported previously for similar (La,Sr)MnO_3/YSZ composite electrodes tested in air [29-32].

4. Conclusions

Chromium substitution for manganese on the B-site of (La,Sr)MnO_3 resulted in lowered σ and raised E_a with regard to electronic conductivity, and raised R_p and E_a associated with the overall ORR. In the case of electronic conductivity, lowered σ and raised E_a may be attributed to a lowering of the number of available small polaron hopping manganese B-sites. Regarding electrochemical oxygen reduction activity, raised R_p and E_a may be attributed to retardation of ORR processes including possibly transport of oxide ions and/or oxygen intermediates across (La,Sr)MnO_3/YSZ interfaces, dissociative adsorption, transfer of species at TPBs, and surface diffusion.

Acknowledgements

The authors thank the Swiss National Science Foundation (SNSF) Indo Swiss Joint Research Programme (ISJRP) for funding (Grant Agreement No. 138 864).

References

[1] S. Taniguchi, M. Kadowaki, H. Kawamura, T. Yasuo, Y. Akiyama, Y. Miyake, T. Saitoh, J. Power Sources 55 (1995) 73.

[2] S.P.S. Badwal, R. Deller, K. Foger, Y. Ramprakash, J.P. Zhang, Solid State Ionics 99 (1997) 297.

[3] S.P. Jiang, J.P. Zhang, L. Apateanu, K. Foger, J. Electrochem. Soc. 147 (2000) 4013.

[4] Y. Matsuzaki, I. Yasuda, J. Electrochem. Soc. 148 (2001) A126.

[5] K. Fujita, T. Hashimoto, K. Ogasawara, H. Kameda, Y. Matsuzaki, T. Sakurai, J. Power Sources 131 (2004) 270.

[6] S.C. Paulson, V.I. Birss, J. Electrochem. Soc. 151 (2004) A1961.

[7] E. Konysheva, H. Penkalla, E. Wessel, J. Mertens, U. Seeling, L. Singheiser, K. Hilpert, J. Electrochem. Soc. 153 (2006) A765.

[8] E. Konysheva, J. Mertens, H. Penkalla, L. Singheiser, K. Hilpert, J. Electrochem. Soc. 154 (2007) B1252.

[9] T. Komatsu, R. Chiba, H. Arai, K. Sato, J. Power Sources 176 (2008) 132.

[10] J.J. Bentzen, J.V.T. Høgh, R. Barfod, A. Hagen, Fuel Cells 9 (2009) 823.

[11] C.J. Fu, K.N. Sun, X.B. Chen, N.Q. Zhang, D.R. Zhou, Electrochim. Acta 54 (2009) 7305.

[12] A. Neumann, N.H. Menzler, I. Vinke, H. Lippert, ECS Trans. 25 (2009) 2889.

[13] N.H. Menzler, I. Vinke, H. Lippert, ECS Trans. 25 (2009) 2899.

[14] J. Wu, C.D. Johnson, R.S. Gemmen, X. Liu, J. Power Sources 189 (2009) 1106.

[15] X. Chen, Y. Zhen, J. Li, S.P. Jiang, Int. J. Hydrogen Energy 35 (2010) 2477.

[16] T. Horita, Y. Xiong, H. Kishimoto, K. Yamaji, M.E. Brito, H. Yokokawa, J. Electrochem. Soc. 157 (2010) B614.

[17] J.A. Schuler, P. Tanasini, A. Hessler-Wyser, C. Comninellis, J. Van Herle, Electrochem. Commun. 12 (2010) 1682.

[18] T. Jin, K. Lu, Int. J. Hydrogen Energy 36 (2011) 4440.

[19] M. Kornely, A. Neumann, N.H. Menzler, A. Leonide, A. Weber, E. Ivers-Tiffée, J. Power Sources 196 (2011) 7203.

[20] J.A. Schuler, C. Gehrig, Z. Wuillemin, A.J. Schuler, J. Wochele, C. Ludwig, A. Hessler-Wyser, J. Van Herle, J. Power Sources 196 (2011) 7225.

[21] H. Yokokawa, T. Horita, N. Sakai, K. Yamaji, M.E. Brito, Y.P. Xiong, H. Kishimoto, Solid State Ionics 177 (2006) 3193.

[22] A. Faes, Z. Wuillemin, P. Tanasini, N. Accardo, J. Van Herle, J. Power Sources 196 (2011) 3553.

[23] R. Shannon, Acta Crystallogr., Sect. A: Found. 32 (1976) 751.

[24] S. Tao, J.T.S. Irvine, Nat. Mater. 2 (2003) 320.

[25] J.A.M. van Roosmalen, J.P.P. Huijsmans, L. Plomp, Solid State Ionics 66 (1993) 279.

[26] M. Mori, N. Sakai, T. Kawada, H. Yokokawa, M. Dokiya, Denki Kagaku 58 (1990) 528.

[27] S.M. Plint, P.A. Connor, S. Tao, J.T.S. Irvine, Solid State Ionics 177 (2006) 2005.

[28] M.J. Jørgensen, M. Mogensen, J. Electrochem. Soc. 148 (2001) A433.

[29] M. Mogensen, S. Skaarup, Solid State Ionics 86–88 (1996) 1151.

[30] E.P. Murray, T. Tsai, S.A. Barnett, Solid State Ionics 110 (1998) 235.

[31] S. Wang, Y. Jiang, Y. Zhang, J. Yan, W. Li, J. Electrochem. Soc. 145 (1998) 1932.

[32] S.R. Gamble, J.T.S. Irvine, Solid State Ionics 192 (2011) 394.